IAHR AIRH

Journal of Hydraulic Research Vol. 43, No. 3 (2005), pp. 234–244

Physical modelling of the flow field in an undular tidal bore

Modélisation physique du champ d'écoulement dans un mascaret ondulé

H. CHANSON MIAHR, Reader, *Department of Civil Engineering, The University of Queensland, Brisbane QLD 4072, Australia. Fax: +61 7 33 65 45 99; e-mail: h.chanson@uq.edu.au*

ABSTRACT
A tidal bore may form in a converging channel with a funnel shape when the tidal range exceeds 6–9 m. The advancing surge has a major impact on the estuarine ecosystem. Physical modelling of an undular bore has been conducted based upon a quasi-steady flow analogy. The experimental data highlight rapid flow redistributions between successive wave troughs and crests as well as large bottom shear stress variations. The results suggest a sediment transport process combining scour beneath wave troughs associated with upward matter dispersion between a trough and the following wave crest. The process is repeated at each trough and significant sediment transport takes place with deposition in upstream intertidal zones. The conceptual model is supported by field observations showing murky waters after the bore passage and long-lasting chaotic waves.

RÉSUMÉ
Un mascaret peut se former dans un canal convergent en forme d'entonnoir quand la hauteur de marée excède 6–9 m. La vague qui avance a un impact important sur l'écosystème de l'estuaire. La modélisation physique d'un mascaret ondulé a été réalisée en se basant sur l'analogie avec un écoulement quasi-stationnaire. Les données expérimentales mettent en lumière des redistributions rapides d'écoulement entre les creux et les crêtes successives des vagues ainsi que des variations importantes du cisaillement au fond. Les résultats suggèrent un processus de transport sédimentaire combinant un affouillement de sédiment sous les creux associé à une dispersion ascendante de matière entre un creux et la crête de vague suivante. Le processus est répété à chaque creux et un transport significatif de sédiment a lieu avec dépôt dans les zones intertidales amont. Le modèle conceptuel est étayé par des observations en nature montrant des eaux troubles après le passage d'un mascaret et des vagues chaotiques durables.

Keywords: Tidal bore, undular bore, undular jump, velocity, pressure, boundary shear stress, sediment process, mixing.

1 Introduction

A tidal bore is a positive surge of tidal origin which may form with large tidal ranges in a converging channel forming a funnel shape. The surge absorbs random disturbances on both sides and this makes the wave stable and self-perpetuating. With appropriate boundary conditions, the bore may travel long distances upstream: e.g., the tidal bore on the Pungue river (Mozambique) is still about 0.7 m high about 50 km upstream of the mouth and it may reach 80 km inland. A tidal bore is basically a series of waves propagating upstream as the tide turns to rising. As the surge progresses inland, the river flow is reversed behind it (e.g., Lynch, 1982; Chanson, 2001). For example, in the Qiantang river (China), fishermen waited for the bore to sail their junks upriver (Tricker, 1965).

Famous examples of tidal bores include the Hangzhou (or Hangchow) bore on the Qiantang river (China), the Amazon river bore called *pororoca* (Brazil),[1] the tidal bore on the Seine river (*mascaret*) (France) and the Hoogly (or Hooghly) bore on the Ganges (India). Smaller tidal bores occur on the Severn river near Gloucester, England, on the Garonne and Dordogne rivers, France, at Turnagain Arm and Knik Arm, Cook Inlet (Alaska), in the Bay of Fundy (at Petitcodiac and Truro), on the Styx and Daly rivers (Australia), and at Batang Lupar (Malaysia) (Figs 1 and 2).

A tidal bore may affect shipping industries. For example, the *mascaret* of the Seine river had had a sinister reputation (Fig. 1a). More than 220 ships were lost between 1789 and 1840 in the Quilleboeuf–Villequier section (Malandain, 1988). The height of the *mascaret* bore could reach up to 7.3 m and the bore front travelled at a celerity of about 2–10 m/s. Even in modern times, the Hoogly and Hangzhou bores are hazards for small ships and boats. Although the Hangzhou bore is a well-known tourist attraction, few dozens of people have been killed every year by river levee overtopping induced by the bore. Tidal bores affect also the estuarine eco-system. The effect on sediment transport was studied at Petitcodiac and Shubenacadie rivers, on the Sée and

[1] One of the first accounts of the *pororoca* was by the Frenchman Charles-Marie LA CONDAMINE (1701–1774) in "Journal du Voyage fait par Ordre du Roi a l'Equateur, servant d'Instruction Historique à la Mesure des Trois Premiers Degrés du Méridien", Imprimerie Royale, Paris, 1751.

Revision received June 30, 2004 / Open for discussion until February, 2006.

(a)

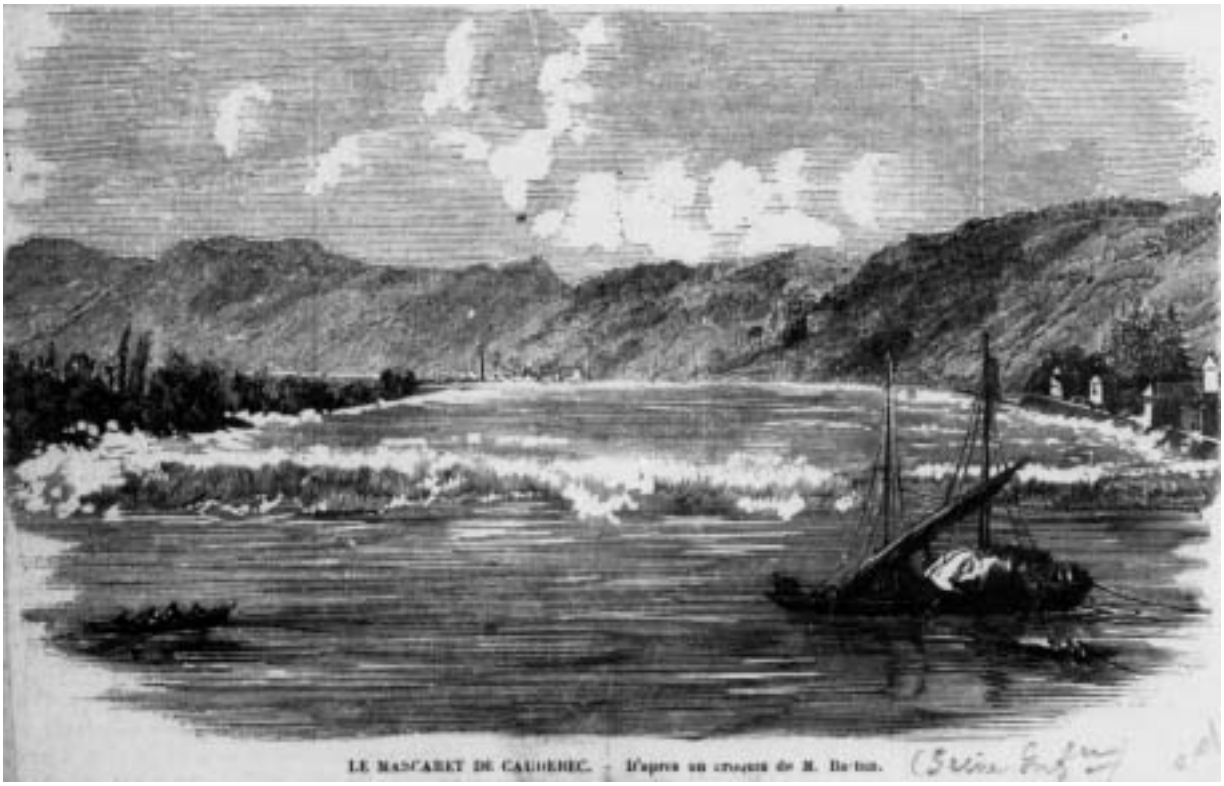

(b)

Figure 1 Field observations of tidal bores. (a) Tidal bore of the Seine river, France—Ancient gravure "Mascaret de Caudebec" by Barbin: "Ils halent le bateau au milieu du fleuve mais il va falloir vite ce mettre face à la barre et la petite embarquation va se faire chahuter!!" (Courtesy of Dr J.J. Malandain). (b) Tidal bore at Batang Lupar (Malaysia) (Courtesy of Mr Lim H.H., Dept of Irrigation & Drainage, Sarawak)—the bore, locally known as "benak", is a danger to shipping in the river. It also causes severe bank erosion. (c) Undular tidal bore of the Couesnon river, Mont-Saint-Michel (France) on 7 March 2004 at sunset—View from Tour Gabriel (right bank), with bore propagation from right to left.

Sélune (Tessier and Terwindt, 1994) and on the Hangzhou bay (Chen *et al.*, 1990). The impact on the ecology is acknowledged in the Amazon where piranhas eat matter in suspension after the passage of the bore, at Turnagain Arm where bald eagles fish behind the bore, in the Severn river (sturgeons in the past, elvers) and in the Bay of Fundy (striped bass spawning).

The best historically documented tidal bores are probably those of the Seine river (France) and Qiantang river (China). The *mascaret* of the Seine river was documented first during the 9th century AD, and in writings from the 11th to 16th centuries (Malandain, 1988). It was locally known as "la Barre". The Qiantang river bore featured in a Chinese novel[2] written in the 16th century and describing historical events from the period

[2]"Outlaws of the Marsh", by Shi Nai'an and Luo Guanzhong. Foreign Languages Press, Beijing 1980.

(c)

Figure 1 (*Continued*)

(a)

Figure 2 Undular tidal bore of the Dordogne river on 27 September 2000 at 5:00 pm (Photographs by the author). (a) Looking downstream at the incoming undular bore. (b) Looking upstream at the murky waters after the bore passage (foreground) and the glossy free-surface in background.

1100–1130 AD. The bore was then known as "The Old Faithful" because it kept time better than clocks. Bartsch-Winkler and Lynch (1988) listed over 80 estuaries experiencing a tidal bore, but it is likely that more are affected.

Despite their impact on estuarine processes, little is known on the flow field, mixing and sediment motion beneath tidal bores. Most observations derived from reports by sailors, fishermen and surfers (e.g., Tricker, 1965). Field measurements are

(b)

Figure 2 (*Continued*)

rare, but Kjerfve and Ferreira (1993) and Wolanski *et al.* (2001). It is the purpose of this paper to gain a new understanding of the impact of undular tidal bores on river systems. The study regroups laboratory experiments based upon the quasi-steady flow analogy performed in a large-size facility with two geometric scaling ratios and some field observation.

2 Methodology

Salient characteristics of tidal bores are revealed in photographs and videos of field occurrences. The writer obtained audiovisual materials on more than 15 tidal bores and he received written information on another 20 bores. First, most tidal bores develop as undular surges characterized by a train of advancing undulations and absence of wave breaking, but close to the banks. For example, Fig. 1(c) shows an undular bore in the Couesnon river; breaking is observed in shallow waters near the banks. Breaking bores are rare, often restricted to king tide conditions and localized in some estuarine sections. For example, the *pororoca* is primarily an undular bore but may break in some shallow water sections of the river mouth (Murphy, 1983). Secondly, before bore arrival, the river flow appears quiet and the free-surface is often smooth and glossy (e.g., Fig. 2b). The inflow conditions are characterized by low turbulence levels.

In absence of detailed field measurements and because numerical models based upon the Saint–Venant equations cannot handle free-surface undulations, a quasi-steady flow analogy was applied to investigate an undular tidal bore with the physical model of an undular jump. The flow conditions were chosen for two series of field observations. Firstly the sighting of the Severn bore by Captain BEECHEY on 1 December 1849 (Tricker, 1965). That is, $d_1 = 1.5$ m and $\mathrm{Fr}_1 = 1.6$, where d_1 is the upstream water depth and Fr_1 is the bore Froude number. Secondly, the observation of the Dordogne river tidal bore on 27 September 2000 with $d_1 \sim 1.5$–2 m and $\mathrm{Fr}_1 \sim 1.3$ (Fig. 2).

Dynamic similarity was achieved by selecting a Froude similitude with undistorted models (e.g., Henderson, 1966; Chanson, 2004). Partially developed inflow conditions were selected to minimize the effects of upstream turbulence: i.e., $\delta/d_1 \sim 0.4$ where δ is the upstream boundary layer thickness (Table 2, column 6). Possible scale effects were investigated with two geometric scales : $L_\mathrm{R} = 19$ and 33 for $\mathrm{Fr}_1 = 1.6$ (i.e., $d_1 = 0.080$ and 0.046 m, respectively) where L_R is the ratio of prototype to model dimensions. For the second Froude number $\mathrm{Fr}_1 = 1.3$, the geometric scaling ratio was 22 (i.e., $d_1 = 0.081$ m).

3 Experimental investigations

New experiments were performed in a rectangular horizontal channel (Table 1, Fig. 3). The flume was 0.5-m wide and 3.2-m long. It was made of smooth PVC bed and glass walls (0.3-m high). The upstream supercritical flow was controlled by a vertical gate and the channel ended with an overflow gate.

The water discharge was measured with a Venturi meter, calibrated *in situ* with a large V-notch weir. The percentage of error was expected to be less than 2%. The water depths were measured using a rail mounted pointer gauge. Pressure, velocity and bed shear stress distributions were recorded with a Prandtl–Pitot tube (3.35-mm external diameter, hemispherical nose). The Pitot tube design is based on the Prandtl design, and it was compared with a British Standards design within 1% in wind tunnel tests for Reynolds numbers ranging from 1×10^5 to 9×10^5. The translation of the gauge and Pitot tube in the direction normal to the channel bottom was controlled by a fine adjustment travelling mechanism (error less than 0.1 mm). The error on the transverse

Table 1 Summary for detailed experimental measurements in undular jump flows

Reference	q (m^2/s)	Fr_1	x_1 (m)	d_1 (m)	δ/d_1	Remarks
Present study						B = 0.5 m. Horizontal channel
Exp. No. HQ1	0.0484	1.58	0.30	0.046	0.43	Vertical sluice gate. Opening: 70 mm
Exp. No. HQ2	0.111	1.57	0.45	0.080	0.42	Vertical sluice gate. Opening: 122.3 mm
Exp. No. CD1	0.0914	1.25	0.35	0.081	0.44	Round gate with upstream flow straighteners. Gate opening: 80 mm

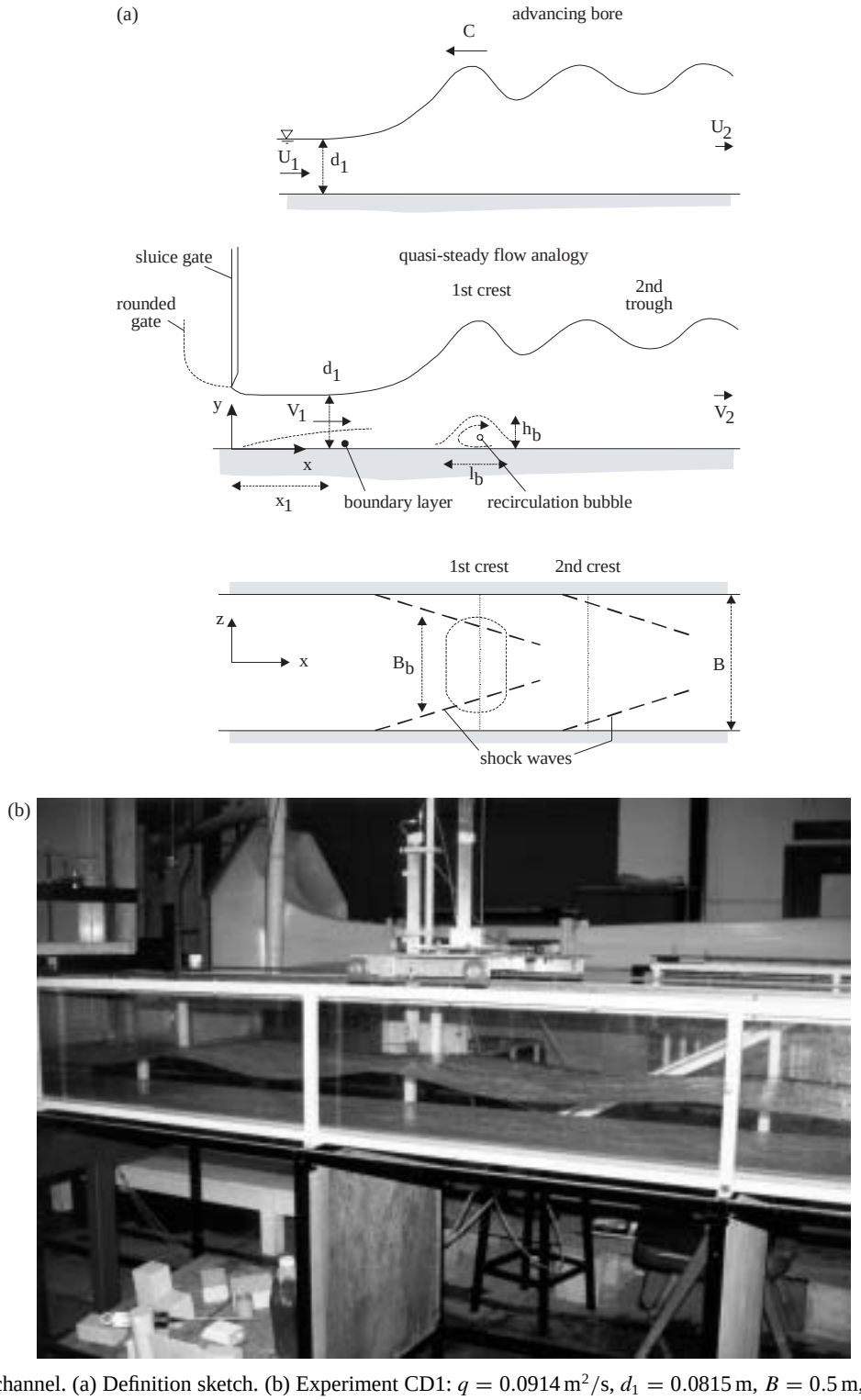

Figure 3 Experimental channel. (a) Definition sketch. (b) Experiment CD1: $q = 0.0914\,m^2/s$, $d_1 = 0.0815\,m$, $B = 0.5\,m$, $Fr_1 = 1.26$ (courtesy of Chantal Donnelly)—Flow from the left to the right. Note the (grey) gate on the far left and the trolley system holding the Pitot tube.

position of the gauge and tube was less than 0.5 mm and the error on their longitudinal position was less than 2 mm.

The Prandtl–Pitot tube was calibrated as a Preston tube based upon *insitu* experiments. The calibration curve was best fitted by:

$$\tau_o = 3.428 * V_b^{1.654} \quad (1)$$

where τ_o is the boundary shear stress and V_b is the velocity measured by the Pitot tube lying on the boundary (Chanson, 2000). Although similar to the calibration curves obtained by Preston (1954), Patel (1965) and Macintosh (1990), Eq. (1) differs quantitatively and the difference was discussed specifically by Chanson (2000). The data accuracy was expected to be about 2% on dynamic and static pressures, 1% on local velocity and 5% on boundary shear stress.

Further details on the experimental facilities were discussed by Chanson (2001) and Donnelly and Chanson (2002).

3.1 Measurement procedure

For each experiment, the inflow conditions were carefully prepared to achieve small bottom boundary layer and low turbulence. Measured boundary layer thicknesses are given in Table 1 (column 6). For each experiment, the upper fluid layer was nearly an ideal flow characterized by low turbulence level (Fig. 3b).

Detailed measurements of free-surface elevation, pressure and velocity distributions were performed at characteristic longitudinal locations: i.e., at wave crests and troughs, and half-distances between crest and trough. At each cross-section, flow properties were recorded at several transverse positions across the channel width to ensure that the flow was two-dimensional (but next to the sidewall) and symmetrical.

4 Experimental results

Visual observations and detailed measurements showed that the undular jump was basically two-dimensional but next to the sidewalls: that is, for $-0.42 < z/B < 0.42$ where z is the transverse distance measured from the centreline and B is the channel width (Table 2, Fig. 4). Table 2 gives dimensionless water depths for one experiment ($Fr_1 = 1.6$) at several longitudinal and transverse positions while Fig. 4 presents the dimensionless free-surface profile for another experiment ($Fr_1 = 1.3$), where x is the distance measured from the gate and d_c is the critical depth.

Small sidewall cross waves were seen upstream of each wave crest. The angle of the crosswaves with the wall was relatively shallow as sketched in Fig. 3(a). Ohtsu *et al.* (1995, 2001) reported a similar observation. For all experiments, a large recirculation bubble was observed below the first crest (Fig. 3a). The recirculation region extended over most of the channel breadth with a maximum height of about $0.47 * d_c$ for the largest Froude number $Fr_1 = 1.6$. Detailed characteristics of the bubble are given in Table 3. A similar recirculation region beneath the first wave crest was described by other researchers investigating undular jumps with partially developed inflow (e.g., Montes, 1986; Ohtsu and *et al.*, 1995; Chanson, 1995).

Figure 5 presents dimensionless pressure and velocity distributions for one experiment ($Fr_1 = 1.6$). The data are compared with an inviscid solution of the Boussinesq equation (Montes and Chanson, 1998). Beneath the undulations, the pressure distributions were not hydrostatic. The pressure gradients were larger than hydrostatic when the free-surface was curved upwards (i.e., *concave*) and less than hydrostatic when the free-surface was *convex*. The trend is predicted by the irrotational flow motion theory (e.g., Rouse, 1938; Liggett, 1994), although greater deviations from hydrostatic pressure distributions were experimentally observed (Fig. 5). At the first wave crest, the velocity distributions differed considerably from theoretical predictions (Fig. 5a). Indeed the flow was affected by the recirculation "bubble". Further downstream, the agreement between data and theory improved slightly. The same trend was observed for all experiments (Table 1).

Dimensionless bottom boundary shear stress data are presented in Fig. 6, where d_c and V_c are the critical depth and velocity, respectively. The results showed consistently maximum boundary shear stresses below wave troughs and minimum values below the crests. Note that the data beneath the first wave crest were affected by the recirculation region (Fig. 3). Large longitudinal

Table 2 Dimensionless free-surface profile : Experiment No. HQ2

x/d_c	d/d_c $z = 0$ (CL)	d/d_c $z/B = 0.144$	d/d_c $z/B = 0.284$	d/d_c $z/B = 0.438$	Remarks
4.17	0.75	0.74	0.74	0.74	Upstream
11.07	0.92	0.91	0.93	0.98	Start of shock wave
16.40	0.99	1.01	1.03	1.05	Between shock and 1st crest
17.70	1.17	1.16	1.13	1.08	At 1st crest
21.68	1.06	1.06	1.08	1.12	Between 1st crest and 1st trough
14.82	1.24	1.19	1.14	1.18	At 1st trough
22.89	1.21	1.26	1.23	1.19	Between 1st trough and 2nd crest
11.77	1.18	1.17	1.20	1.23	At 2nd crest
20.38	1.30	1.25	1.26	1.31	Between 2nd crest and 2nd trough
13.25	1.45	1.47	1.44	1.39	At 2nd trough
19.04	1.55	1.56	1.60	1.49	Between 2nd trough and 3rd crest
24.09	1.55	1.51	1.49	1.52	At 3rd crest

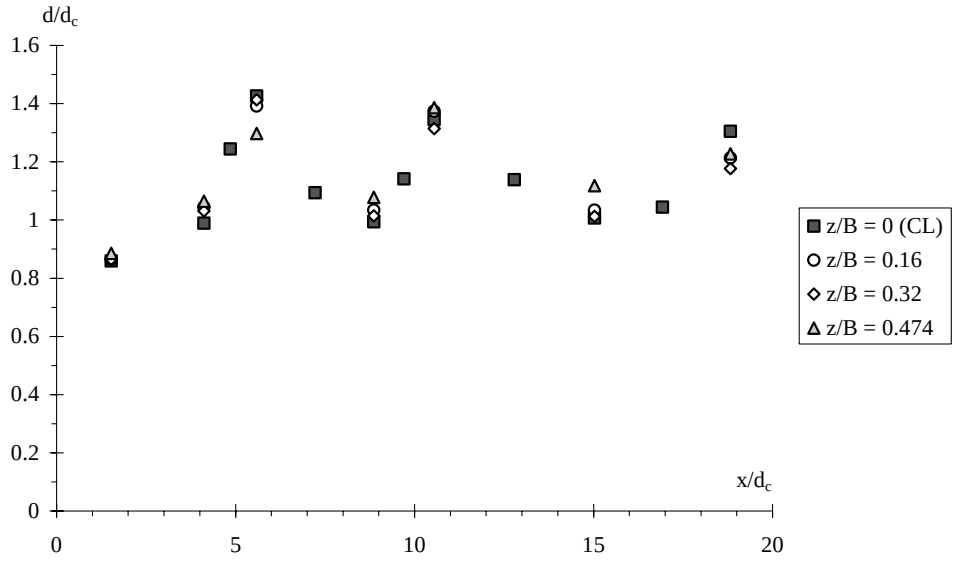

Figure 4 Dimensionless free-surface profile for $Fr_1 = 1.3$ (experiment CD1).

Table 3 Characteristics of the recirculation region beneath the first wave crest

Reference	Fr_1	d_{1C} (m)	h_b (m)	B_b (m)	l_b (m)	Remarks
Present study						B = 0.5 m. Horizontal channel
Exp. No. HQ1	1.58	0.095	0.03	0.44	0.05	Vertical sluice gate. Opening : 70 mm
Exp. No. HQ2	1.57	0.158	0.05	0.40	0.10	Vertical sluice gate. Opening : 122.3 mm
Exp. No. CD1	1.25	0.1353	0.01	0.40	0.05	Round gate with upstream flow straighteners. Gate opening : 80 mm

Notes : d_{1C}: centreline water depth at first crest; h_b : recirculation bubble maximum height; B_b : recirculation bubble width; l_b : recirculation bubble maximum length.

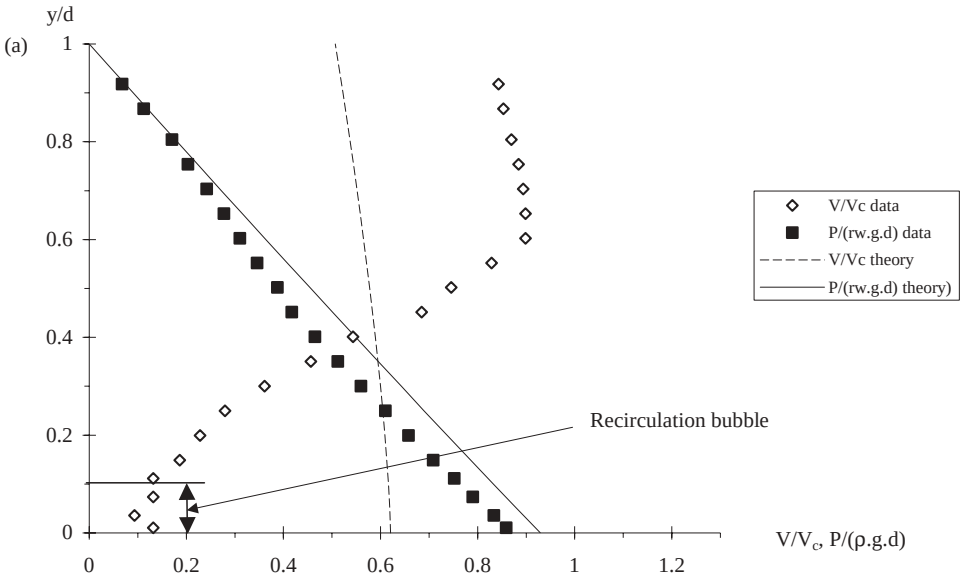

Figure 5 Dimensionless pressure and velocity distributions: comparison with inviscid Boussinesq theory (Montes and Chanson, 1998)—$Fr_1 = 1.6$, Exp. No. HQ2 centreline data. Legend: Black square $= P/\rho_w^* g^* d$; White diamond $= V/V_c$. (a) First wave crest. (b) First wave trough. (c) Second wave crest. (d) Second wave trough.

variations of shear stress were observed beneath the undulations: e.g., in Fig. 6, the boundary shear stress below the second trough is about twice of that observed at the second and third wave crest. A comparison of Chanson's (2000) and present results suggests that the time-averaged, maximum bed shear stress, beneath wave trough, was about:

$$\frac{(\tau_o)_{max}}{0.5 * \rho * V_c^2} \sim 0.0045 \quad (2)$$

while time-averaged, minimum bed shear stress, beneath wave crests, was about:

$$\frac{(\tau_o)_{min}}{0.5 * \rho * V_c^2} \sim 0.0015 \quad (3)$$

where ρ is the fluid density.

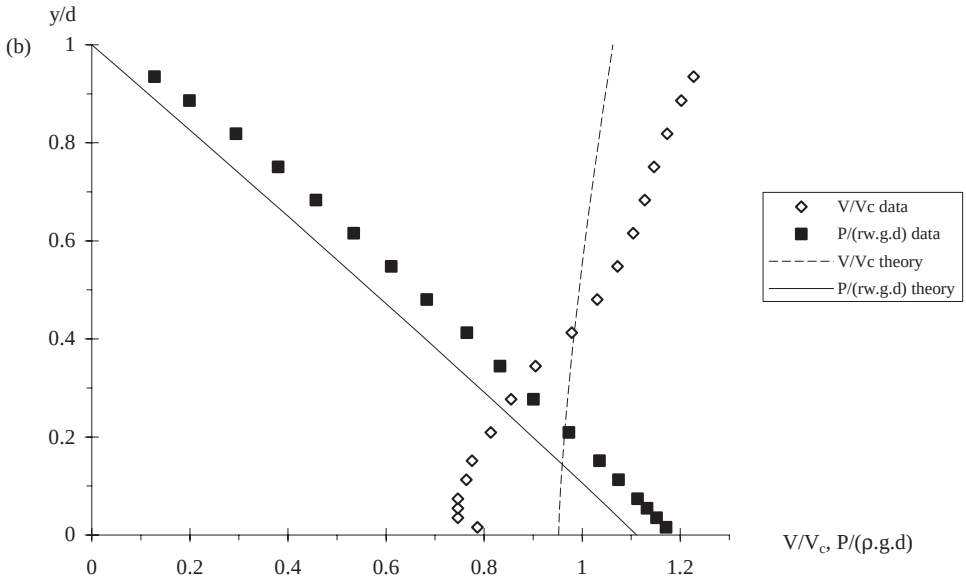

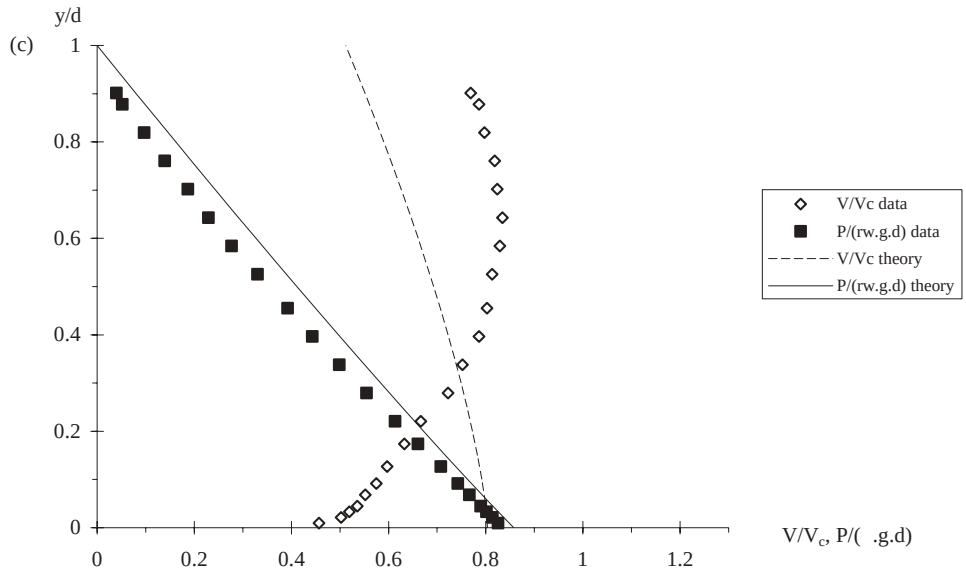

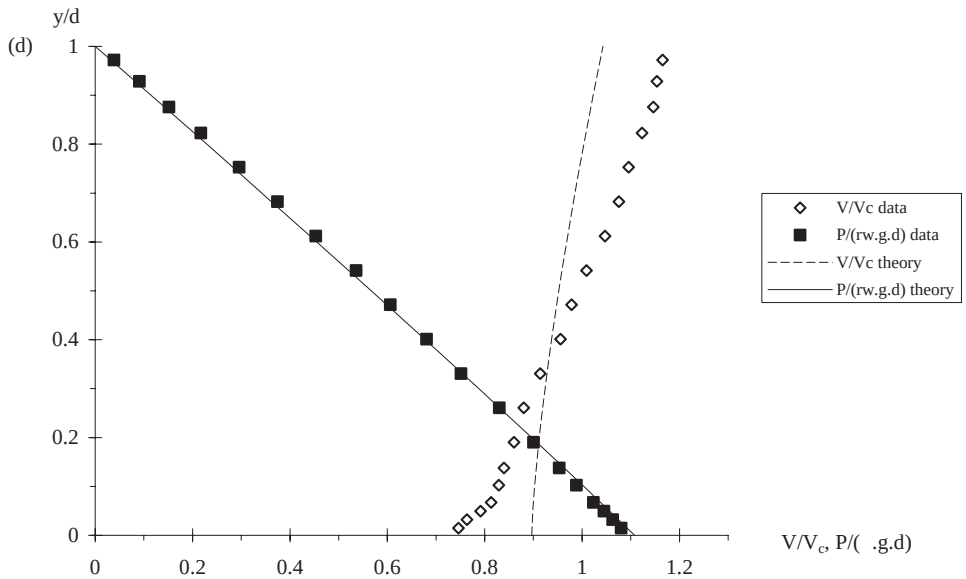

Figure 5 (*Continued*)

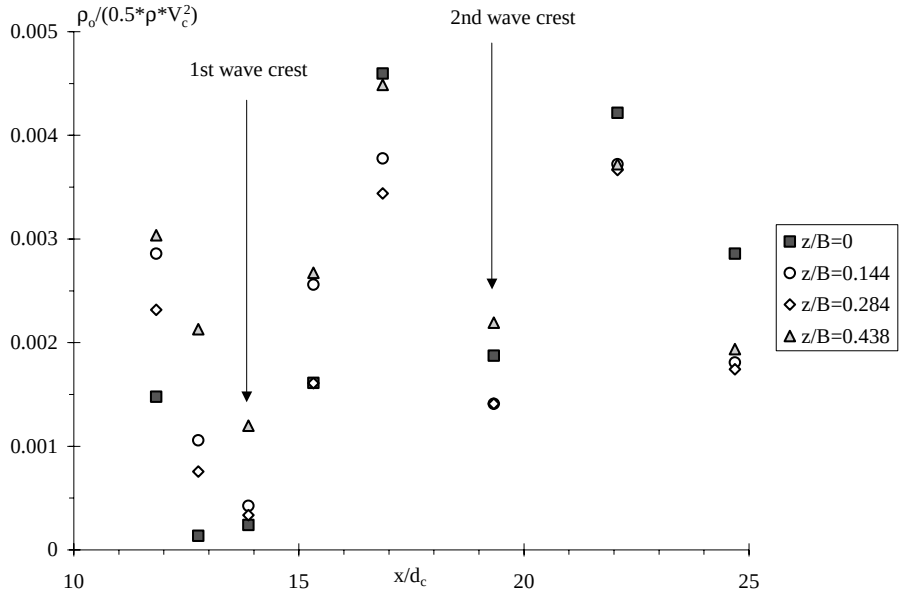

Figure 6 Dimensionless bottom boundary shear stress $\tau_o/(\rho * V_c^2/2)$ as a function of the dimensionless longitudinal distance x/d_c ($Fr_1 = 1.6$, Exp. No. HQ2).

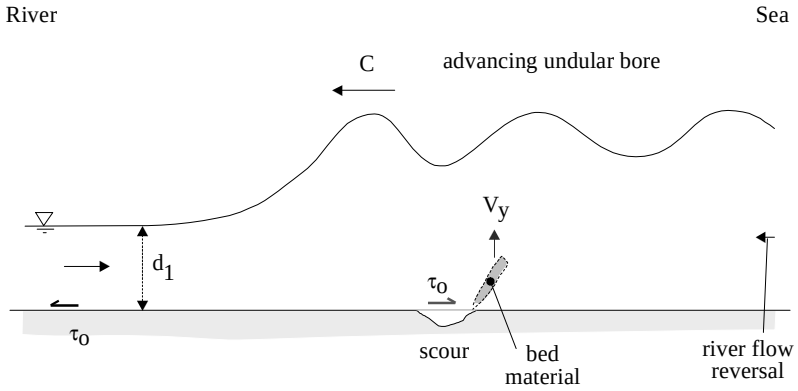

Figure 7 Sketch of sediment bed scour and dispersion at an undular tidal bore.

4.1 Discussion

For identical inflow conditions ($Fr_1 = 1.6$, $\delta/d_1 = 0.4$), experimental data obtained with two geometric scales ($d_1 = 0.046$ and 0.080 m) showed nearly identical dimensionless pressure and velocity distributions upstream and beneath the undulations, but close to the wall. The result suggests that scale effects were negligible.

For one experiment ($Fr_1 = 1.3$), detailed velocity and pressure measurements were conducted on either side of a crest and a trough: i.e., at half-distance between crest and trough. The results showed consistently an absence of symmetry. There was no exact correspondence in shape and magnitude, on opposite sides of a crest or trough. Velocity data showed a greater flow acceleration next to the bottom (i.e., $y/d_c < 0.3$), between crest and trough, than the corresponding deceleration between trough and crest.

5 Practical applications

5.1 Applications to tidal bores

Present results may be applied to an advancing undular tidal bore using the quasi-steady flow analogy. Considering an undular surge progressing upstream, the river bed is subjected to a rapid flow reversal at the wave front associated with bottom shear stress reversal and maximum (negative) boundary shear stress beneath the troughs (Figs 6 and 7). This pattern suggests some scour beneath the first wave trough while sediment matter is carried upwards by vertical flow motion occurring between the trough and the following wave crest. Experimental data and ideal flow calculations yielded depth-average vertical velocity component V_y of about $+0.10 * V_c$ and $+0.12 * V_c$ between trough and wave crest for $Fr_1 = 1.3$ and 1.6, respectively.[3] For the flow conditions shown in Fig. 2, it yields $V_y = +0.4$ m/s. Downstream of the first wave trough, further scour and sediment dispersion continue beneath the following undulations. Fine sediment materials (silt, clay) are put into suspension and transported upstream with the bore. Ultimately they are deposited in intertidal zones. The resuspension of matter behind the bore may have serious implications in rivers such as the Mersey, UK, where the bore may resuspend heavy toxic metals and industrial wastes sunk into the river bed.

[3]For a tidal bore, the critical velocity is calculated based upon the continuity equation for the quasi-steady flow (Henderson, 1966, p. 76, Eqs (3)–(15); Chanson, 1999, p. 69, Eqs (4)–(9a)).

Figure 2 shows the tidal bore of the Dordogne river at St Pardon, France, about 103 km upstream of Pointe de Grave on 27 September 2000 (coefficient: 103). At that location, the river is about 350 m wide and there is no sharp bend for about 3–4 km. The initial water depth was about 1.5–2 m. In September 2000, the bore exhibited about 8–12 well-formed undulations with a wave height of about 1 m and wave length of about 8 m for an inflow surge Froude number $\mathrm{Fr}_1 \sim 1.3$ (Fig. 2). The undulations were followed by irregular waves. Two dominant features of the bore were the murkiness of the water after the passage of the bore, and the chaotic wave motion lasting for some time. The former highlights significant sediment motion at the bore front, even with an undular bore, and this was reported at the Hangzhou, Petitcodiac, Rio Mearim and Severn bores for example. In Fig. 2(b), the waters are dark brown behind the surfers while some black sediment matter is seen on the bottom right as a result of bed material advection to the free-surface by large-scale turbulence. The latter effect (i.e., long-lasting chaotic wave motion) was not well documented. In September 2000, the long-lasting wave motion made difficult for surfers to come back on shore even 20–30 min after the passage of the bore. Such a wave motion contributes further to keep fine material in suspension behind the bore (e.g., Nielsen, 1992). In the Seine river, the waves following the bore were called "*éteules*" and H.L. Partiot[4] sketched them in 1860 (Malandain, 1988, p. 37).

Note, for completeness, that some researchers observed a related chaotic wave motion, propagating as far as $(x - x_1)/d_c \sim 2{,}000$, downstream of undular jumps in laboratory and in man-made canals: e.g., Darcy and Bazin (1865) in the Canal de Bourgogne, Chanson (1995) in a 20-m long channel.

5.2 Limitations of the physical modelling

The application of the undular jump results has some limit. During the experiments, very rapid changes in velocity and pressure distributions were observed upstream of and at the first wave crest. A number of researchers reported similar observations in undular hydraulic jumps and it was demonstrated that the flow field is strongly affected by bottom and sidewall boundary friction (e.g., Montes and Chanson, 1998). It is felt that the shear-dominated flow redistribution at the first wave crest is likely to be specific to undular hydraulic jumps and it might not be observed in undular positive surges.

Field observations showed significant sediment motion (Figs 1 and 2). Present experiments were conducted with a fixed boundary channel, neglecting bed scour and interactions between suspended matter and turbulence.

6 Summary and conclusion

The occurrence of tidal bores has a significant impact on river ecosystems while man-made constructions may affect the tidal process. For example, the tidal bores of the Seine (France) and Colorado (USA) rivers disappeared almost completely after major river training, while the bores of the Petitcodiac (Canada) and Couesnon (France) rivers nearly vanished after construction of an upstream dam.

Visual observations suggested that the most common occurrence of tidal bores is in the form of an undular surge (Figs 1 and 2). Physical modelling of an undular bore has been conducted based upon a quasi-steady flow analogy for two geometric scales and two inflow Froude numbers. Detailed velocity and pressure distribution measurements highlighted rapid pressure and velocity re-distributions between successive wave crests and troughs, associated with large longitudinal variations of bottom shear stress. The results, applied to undular tidal bores, suggest that bed erosion and scour take place beneath wave troughs, and that matters are carried upwards between a trough and the following wave crest (Fig. 7). The process is repeated at each undulation and it contributes to significant sediment transport with deposition in upstream intertidal areas. Such a conceptual model is confirmed by field observations showing murky waters after the bore passage. Long-lasting chaotic waves were also observed behind the bore and these contributed to further dispersion of sediments.

Acknowledgments

The writer acknowledges the assistance of K. Hickox, C. Quinlan, C. Donnelly and Y.H. Chou (Australia). He thanks also Dr S. Aoki (Japan), Mr Lim Hiok Hwa (Malaysia), Dr J.E. Jones (UK), Mr D. Leblanc (Canada), Mrs N. Lemiere (France), Dr J.J. Malandain (France), Mr D. Thiedermann (USA), the Bore Ryders Club (UK) and many more people for providing him with new material of interest.

Notation

B = Channel width (m)
B_b = Recirculation bubble width (m)
C = Surge celerity (m/s) as seen by an observer standing on the channel bank
d = Flow depth (m) measured perpendicular to the channel bottom
d_c = Critical flow depth (m): for a rectangular channel: $d_c = \sqrt[3]{q^2/g}$
d_1 = Flow depth (m) measured immediately upstream of the hydraulic jump
Fr = Froude number
Fr_1 = Upstream Froude number: $V_1/\sqrt{g * d_1}$; for a positive surge: $(U_1 + C)/\sqrt{g * d_1}$
g = Gravity constant: $g = 9.80$ m/s^2 in Brisbane, Australia
h_b = Recirculation bubble maximum height (m)
L_R = Geometric scaling ratio of prototype to model dimensions
l_b = Recirculation bubble maximum length (m)
P = Pressure (Pa)
q = Water discharge per unit width (m^2/s)
U_1 = Flow velocity (m/s) upstream of a bore

[4] "*Mémoire sur le Mascaret*", *Annales des Ponts et Chaussées*, 1861.

V = Velocity (m/s)
V_b = Velocity (m/s) measured next to the bed
V_c = Critical velocity (m/s)
x = Longitudinal distance (m) measured along the channel bottom
x_1 = Distance (m) between the channel intake and the jump upstream flow location (where d_1 is measured)
y = Distance measured perpendicular to the channel bed surface (m)
z = Distance (m) across the channel width measured from the centreline
δ = Boundary layer thickness (m)
ρ = Water density (kg/m^3)
τ_o = Boundary shear stress (Pa)

Other symbol
$\oslash$ = Diameter (m)

Subscript
CL = On the flume centreline
c = Critical flow conditions
i_C = i-th wave crest
y = Vertical component
1 = 1—flow conditions upstream of the hydraulic jump
2—initial flow conditions of a positive surge
2 = 1—flow conditions downstream of the hydraulic jump
2— new flow conditions after the passage of a positive surge
1C = First wave crest

References

1. BARTSCH-WINKLER, S. and LYNCH, D.K. (1988). "Catalog of Worldwide Tidal Bore Occurrences and Characteristics". *US Geological Survey Circular*, No. 1022, 17 pp.
2. CHANSON, H. (1995). "Flow Characteristics of Undular Hydraulic Jumps. Comparison with Near-Critical Flows". *Report CH45/95*, Department of Civil Engineering, University of Queensland, Australia, 202 p.
3. CHANSON, H. (2000). "Boundary Shear Stress Measurements in Undular Flows: Application to Standing Wave Bed Forms". *Water Res. Res.* 36(10), 3063.
4. CHANSON, H. (2001). "Flow Field in a Tidal Bore: a Physical Model". *Proceedings of the 29th IAHR Congress*, Beijing, China, Theme E, Tsinghua University Press, Beijing, G. LI Ed., pp. 365–373.
5. CHANSON, H. (2004). *The Hydraulics of Open Channel Flows: an Introduction*, 2nd edn. Butterworth-Heinemann, London.
6. CHEN, J., LIU, C., ZHANG, C. and WALKER, H.J. (1990). "Geomorphological Development and Sedimentation in Qiantang Estuary and Hangzhou Bay". *J. Coastal Res.* 6(3), 559.
7. DARCY, H.P.G. and BAZIN, H. (1865). *Recherches Hydrauliques*. Imprimerie Impériales, Paris, Parties 1ère et 2ème.
8. DONNELLY, C. and CHANSON, H. (2002). "Environmental Impact of a Tidal Bore on Tropical Rivers". *Proceedings of the 5th International River Management Symposium*, 3–6 September Brisbane, Australia, 9 pp.
9. HENDERSON, F.M. (1966). *Open Channel Flow*. MacMillan Company, New York.
10. KJERFVE, B. and FERREIRA, H.O. (1993). "Tidal Bores: First Ever Measurements". *Ciência e Cultura (J. Brazilian Assoc. Advancement Sci.)* 45(2), March/April, 135–138.
11. LIGGETT, J.A. (1994). *Fluid Mechanics*. McGraw-Hill, New York.
12. LYNCH, D.K. (1982). "Tidal Bores". *Scientific American* 247(4), Oct., 134–143.
13. MACINTOSH, J.C. (1990). "Hydraulic Characteristics in Channels of Complex Cross-Section". PhD Thesis, Department of Civil Engineering, University of Queensland, Australia, 487 pp.
14. MALANDAIN, J.J. (1988). "La Seine au Temps du Mascaret". *Le Chasse-Marée*, No. 34, pp. 30–45.
15. MONTES, J.S. (1986). "A Study of the Undular Jump Profile". *Proceedings of the 9th Australasian Fluid Mechanics Conference AFMC*, Auckland, New Zealand, pp. 148–151.
16. MONTES, J.S. and CHANSON, H. (1998). "Characteristics of Undular Hydraulic Jumps. Results and Calculations". *J. Hydraul. Engng.*, ASCE 124(2), 192–205.
17. MURPHY, D. (1983). "Pororoca !." *Calypso Log*, Cousteau Society, 10(2) June, 8–11.
18. NIELSEN, P. (1992). *Coastal Bottom Boundary Layers and Sediment Transport*. Advanced Series on Ocean Engineering, Vol. 4. World Scientific, Singapore.
19. OHTSU, I., YASUDA, Y. and GOTOU, H. (1995). "Characteristics of Undular Jumps in Rectangular Channels". In: ERVINE, D.A. (ed.) *Proceedings of the 26th IAHR Congress*, London, UK, Vol. 1, Paper 1C14, pp. 450–455.
20. OHTSU, I., YASUDA, Y. and GOTOH, H. (2001). "Hydraulic Condition for Undular-Jump Formations". *J. Hydraul. Res.*, IAHR 39(2), 203–209.
21. PATEL, V.C. (1965). "Calibration of the Preston Tube and Limitations on its use in Pressure Gradients". *J. Fluid Mech.* 23(Part 1), Sept., 185–208.
22. PRESTON, J.H. (1954). "The Determination of Turbulent Skin Friction by Means of Pitot Tubes". *J. R. Aeronaut. Soc., London* 58(Feb.), 109–121.
23. ROUSE, H. (1938). *Fluid Mechanics for Hydraulic Engineers*. McGraw-Hill Publishers, New York.
24. TESSIER, B. and TERWINDT, J.H.J. (1994). "An Example of Soft-Sediment Deformations in an Intertidal Environment—The Effect of a Tidal Bore". *Comptes-Rendus de l'Académie des Sciences*, Série II, 319(2), Part 2, 217–233.
25. TRICKER, R.A.R. (1965). Bores, Breakers, Waves and Wakes. *American Elsevier Publ. Co.*, New York.
26. WOLANSKI, E., MOORE, K., SPAGNOL, S., D'ADAMO, N. and PATTIERATCHI, C. (2001). "Rapid, Human-Induced Siltation of the Macro-Tidal Ord River Estuary, Western Australia". *Estuar. Coast. Shelf Sci.* 53, 717–732.